



D2.1 | DOS measurements

Authors: Elia Strambini, Nadia Ligato

Delivery date: 24.10.2019

Version: 3.0



Project Acronym:	SUPERTED
Project Full Title:	Thermoelectric detector based on superconductor-ferromagnetic heterostructures
Call:	H2020-FETOPEN-2016-2017
Topic:	FETOPEN-01-2016-2017
Type of Action:	RIA
Grant Number:	800923
Project URL:	https://superted-project.eu/

Editor:	Nadia Ligato, CNR; Elia Strambini, CNR
Deliverable nature:	Report (R)
Dissemination level:	Public (PU)
Contractual Delivery Date:	31.8.2019
Actual Delivery Date:	24.10.2019
Number of pages:	20
Keywords:	superconducting thermoelectric detector, ferromagnetic insulator-superconductor heterostructures, tunneling spectroscopy, spin-splitting
Authors:	Nadia Ligato, CNR Elia Strambini, CNR
Contributor(s):	Tero Heikkilä, JYU Heli Lehtivuori, JYU
External contributor(s):	Mikel Rouco, CFM

Abstract

Deliverable 2.1 ‘*DOS measurements*’ belongs to the Work Package 2, in which superconducting thermoelectric detectors will be made, and their thermodynamic properties will be characterized. It presents sheet resistance and tunneling spectroscopy measurements, performed during the first 12 months of the project (September 2018 – August 2019), revealing the hybridization of the insulator-superconductor (FI/S) heterostructures. The aim of our tunneling conductance experiments is to explore the presence of the expected spin-splitting superconducting density of states (DOS) due to the exchange field induced by the adjacent insulator.



1. Introduction

A central step to realize the superconducting thermoelectric detector of SUPERTED project is to fabricate ferromagnetic insulator-superconductor (FI/S) heterostructures, where the FI has a double functionality: on the one hand, to induce a spin-splitting field in the adjacent superconductor layer via the magnetic proximity effect [1], on the other hand to generate a spin selective tunnel barrier via the FI layer. The spin-splitting in the quasiparticle density of states (DOS) becomes clearly observable when the magnetic domains of the FI are larger than the superconducting coherence length, ξ [2]. This is the case of the europium sulfide/aluminum (EuS/Al) systems [3], where the magnetic domains of the EuS film can be of the order of a micrometer [4], while the Al layer with a thickness of few nanometers has a coherence length ~ 100 nm. Other necessary conditions to obtain a large spin-splitting depend on the intrinsic properties of the superconductor. For example, a sizeable spin-splitting has been observed in materials with low spin-orbit scattering rate, i.e. materials with relative low atomic number Z , such Al and vanadium (V), while for heavier materials, such as niobium (Nb) and lead (Pb), the strong spin-orbit coupling leads to a lower or absent spin-splitting [5]. At present, Eu chalcogenide (EuS, EuSe) layers in contact with Al thin films are the best materials combination for the realization of superconducting hybrid structures with a large and clear visible spin-splitting [6-8]. Here, we present sheet resistance and tunneling spectroscopy measurements revealing the hybridization of EuS/Al films. The aim of our tunneling conductance experiments is to explore the presence of the expected spin-splitting Al DOS due to the exchange field induced by the EuS.

In the first part of this Deliverable, we report tunneling spectroscopy results performed on N/FI/S tunnel junctions provided by the collaboration with Dr. Jagadeesh S. Moodera [8,9] from Massachusetts Institute of Technology (MIT), USA. Dr. Moodera, together with Dr. Paul Tedrow and Dr. Bob Mersevey, is one of the pioneers of the EuS/Al-based technologies [10-12] and he is still very active within this field of research. From these measurements, we can quantify both the exchange interaction induced by EuS in the Al layer and the degree of spin filtering obtained via the EuS tunnel barrier. Tunneling spectroscopy is performed by measuring the current-voltage (I - V) characteristics in a DC two-wire set-up from which the differential conductance, dI/dV , is determined via numerical differentiation.

In the second part, we present the electrical characterization of EuS/Al films provided by the CFM (Material Physics Center, San Sebastian, Spain), the partner of the consortium in charge to establish a new guideline for the growth of FI/S films, independent of any external collaboration. The temperature (T) dependence of the sheet resistance of samples (FI/S and FI/S/FI films) allows to determine the critical temperature (T_c) of the superconducting films. The strong relation of T_c with the FI layer thickness and the polarization demonstrates a successful magnetization of the Al film induced by the EuS layer showing also a good ferromagnetic hysteresis.

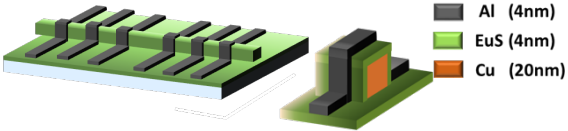
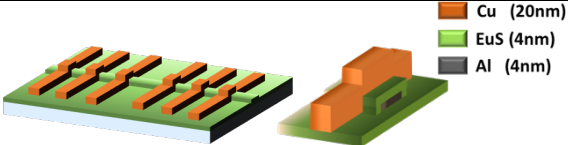
All the measurements are performed at cryogenic temperatures in a filtered cryogen-free dilution refrigerator, with typical RC filter resistance $\sim 2\text{k}\Omega$ (NEST labs, CNR-NANO, Pisa, Italy).



2. Moodera's samples

In this section, we report the results of the tunneling spectroscopy performed on N/FI/S and S/FI/N tunnel junctions provided by the collaboration with Dr. J. Moodera. Experimentally, we have measured the tunneling conductance of the junctions as a function of an applied voltage V_{bias} and an external magnetic field, in order to investigate the induced spin-splitting in the superconductor-ferromagnetic insulator structures and the degrees of spin filtering of the EuS tunnel barrier. The samples consist of two different families of Cu(20 nm)/EuS(X)/Al(4 nm) tunnel junctions, distinguished by the position of the Cu lead (bottom or top) and the thickness of the EuS tunnel barriers (X = 2 nm and 4 nm). The fabrication characteristics of the two families of the investigated samples are reported in Table 1.

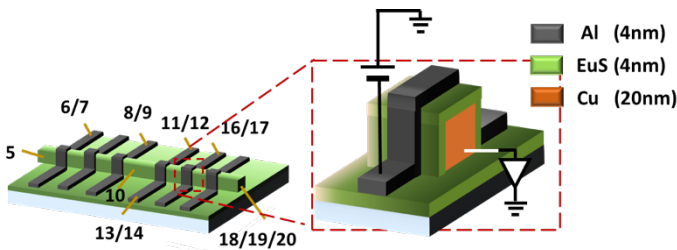
Table 1. Overview of the fabrication characteristics

Sample	Materials/thicknesses	Sketch of the samples
10233-40ÅG	Al(4 nm)/EuS(4 nm)/Cu(20 nm)/glass Al ₂ O ₃ (13nm) on top of Al	
10222-20Å/A	Cu(20 nm)/EuS(2 nm)/Al(4 nm)/glass Al ₂ O ₃ (13nm) on top of Cu	

2.1 Sample 10233-40ÅG

The sample 10233-40ÅG consists of cross bars fabricated by electron-beam shadow mask evaporation. The typical area of Al/EuS/Cu junction is 300x300 μm^2 . The measurement set-up used is shown in Fig. 1. The value of the tunnel resistances measured at 300 K and 30 mK are reported in Table 1b.

a)



b)

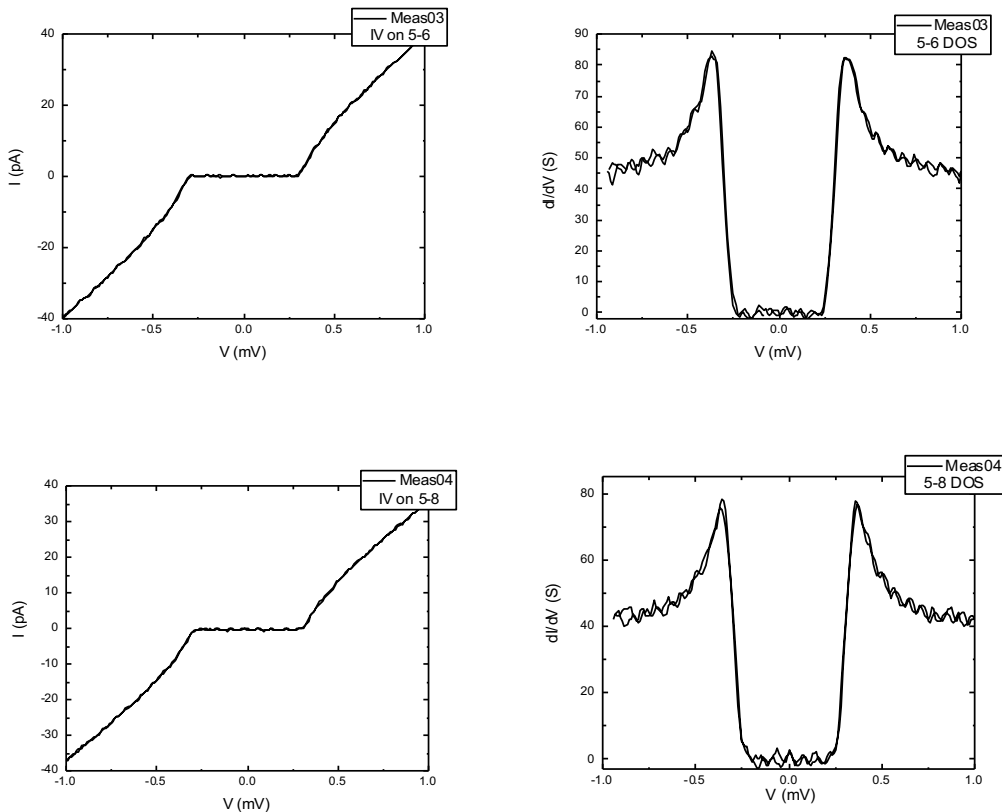
Pins	$R_{300\text{K}}$ (k Ω)	$R_{30\text{mK}}$ (M Ω)
5-6	4.3	20
5-8	5.9	20
5-16	6.5	20
5-11	6.1	20

Figure 1. (a) Sketch and measurement set-up of the device investigated with pinning numbers and a magnification of the cross bar forming the Al/EuS/Cu vertical junction. (b) Tunnel resistances measured at $T = 300$ K and 30 mK. The large difference between the resistances at room T and low T is due to the semiconductor to ferromagnetic-insulator transition of the EuS expected below a Curie temperature of 17 K.



2.1.1 Tunneling spectroscopy before the application of a magnetic field

A base characterization of the Al/EuS/Cu sample in a non-polarized environment are shown in this section. Experimentally, we have measured the current-voltage (I - V) curves and extracted the tunneling conductance via numerical differentiation as a function of V_{bias} and in absence of an external magnetic field. All measurements were performed at 25 mK in a DC two-wire configuration on the couple of pins labelled in each panel and referring to the map reported in Figure 1. Before the magnetization of the EuS layer, an exchange spin splitting in the DOS of the superconducting film is visible only if the ferromagnetic insulator consists of domains larger than the superconducting coherence length, ξ [2]. In the opposite case, the exchange interaction induced on the superconductor by the random orientation of EuS magnetic domains is averaged and the spin-splitting in the density of states is not visible. This is the case of our sample. Figure 2 reports the acquired I - V characteristics of the junctions and the extracted $dI/dV(V)$ as function of the V_{bias} . All Al/EuS/Cu junctions show tunnel characteristics with negligible sub-gap conductance and coherence peaks at the gap voltage of 350 μV , without spin-splitting features.



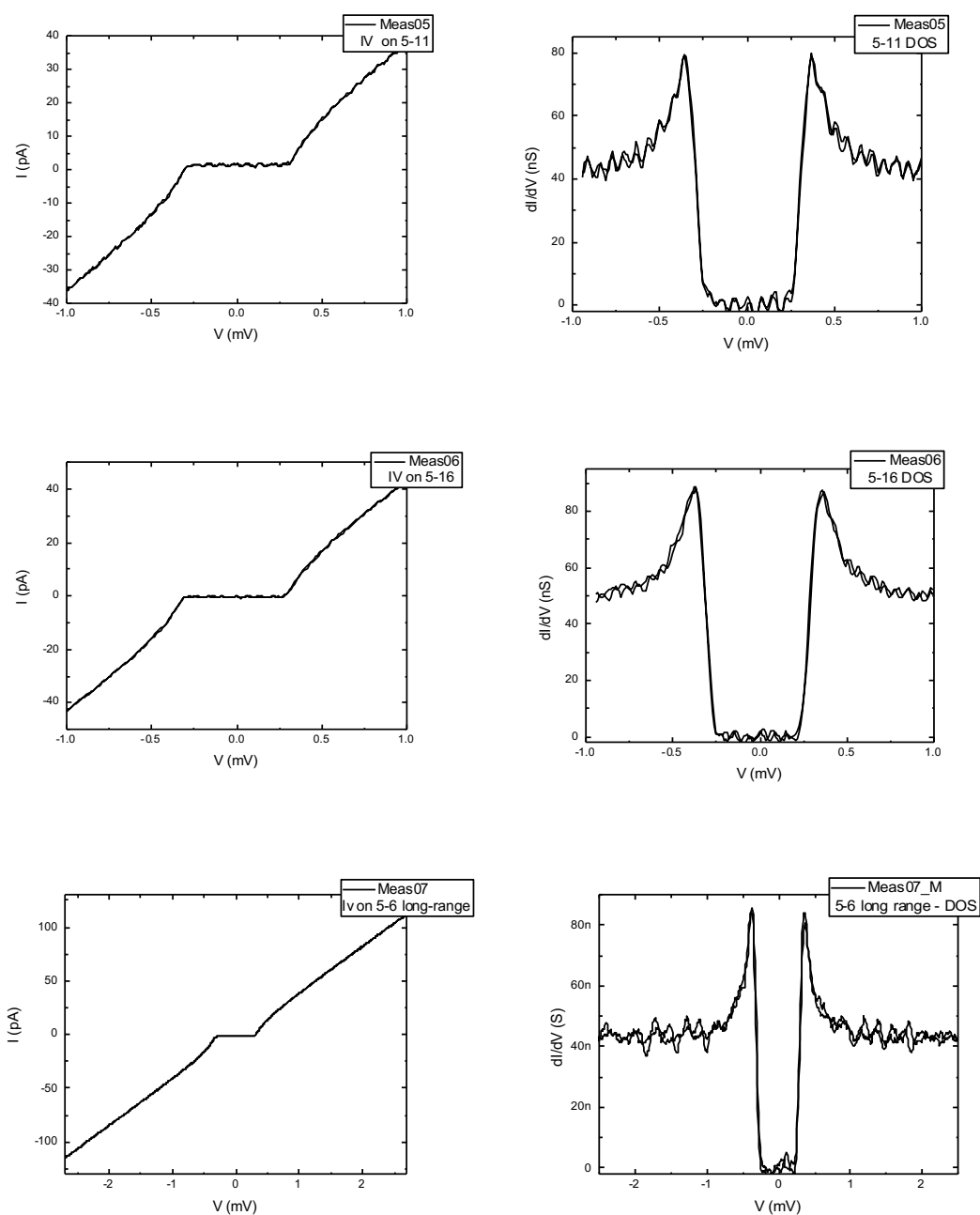


Figure 2. The I - V curves (left panel) and the differential conductance characteristics (right panel) of the Al/EuS/Cu junctions at zero magnetic field.



2.1.2 Tunneling spectroscopy after the application of a magnetic field

Now we report the main results obtained when a magnetic field is applied. Experimentally, we have applied an in-plane magnetic field strong enough (> 44 mT) to obtain the first magnetization of the EuS layer. Unless explicitly reported, all measurements have been performed on the junction with pinning numbers 5-6 (see Figure 1). The results are reported in Figure 3, where we show the differential conductance obtained by the numerical differentiation of the measured I - V characteristics of the junction in a magnetic environment ($B = 150$ mT). Differently from the previous results, the polarization of the EuS is now clear with the asymmetry of the $dI/dV(V)$ curve and the presence of four-peak structures.

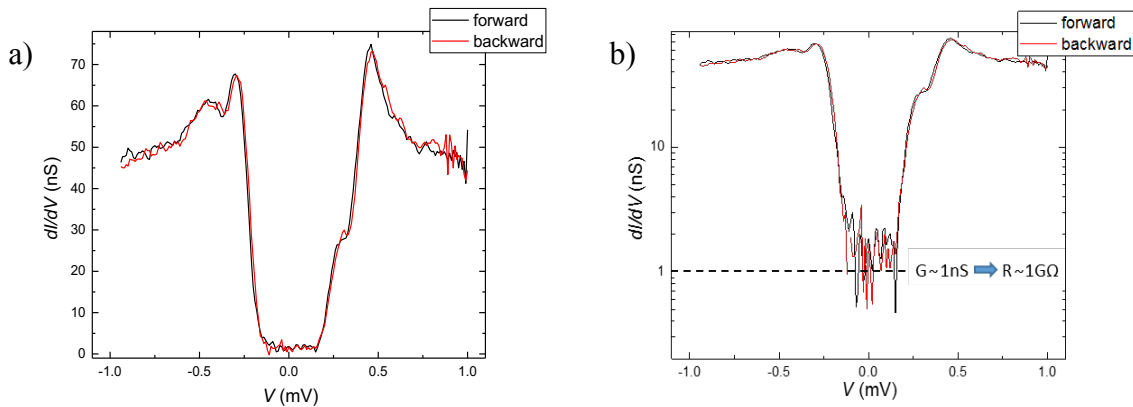


Figure 3. (a) Differential conductance of the Al/Eu/Cu junction (pinning numbers 5-6) as a function of the V_{bias} , for an applied magnetic field $B = 150$ mT. The panel (b) reports $dI/dV(V)$ characteristics in log scale. The dashed line ($R_{\text{tunnel}}(V = 0) \sim 1$ G Ω) reports the junction impedance.

2.1.3 Magnetic field dependence of the tunneling conductance

Here, we focus on the dependence of the $dI/dV(V)$ with the in-plane magnetic field that allows to evaluate the evolution of the local magnetization and spin-splitting from zero (see Figure 2) to its maximum value (see Figure 3). In panel a) of Figure 4, we report the full evolution of the differential conductance obtained by a numerical differentiation of the I - V acquired as a function of the applied V_{bias} and varying the applied magnetic field from -150 mT to 150 mT. At high magnetic fields four peaks are clearly visible in the spectrum of the tunneling conductance, stemming from the splitting of the two Bardeen-Cooper-Schrieffer (BCS) divergence peaks in the two spin projections (see the blue solid curve in Figure 4b). In the same panel a clear asymmetry in the bias voltage is also evident demonstrating a different resistance of the EuS barrier for the two spin species. At zero magnetic field the spin-splitting is not resolved while a small asymmetry in the curve is present (see green solid curve in Figure 4b) suggesting a weak ferromagnetism of the EuS layer or a reduction of the domain sizes. The asymmetry is completely resolved at 44 mT corresponding to the coercive field of the EuS layer.



By fitting these experimental data, we extract for the FI tunnel barrier a polarization of $\sim 50\%$ at 140 mT and an exchange energy of $75 \mu\text{eV}$. The splitting decreases by lowering the magnetic field with a remanent exchange splitting of $20 \mu\text{eV}$ at zero and no splitting at 44 mT due to the switching of polarization of the EuS layer.

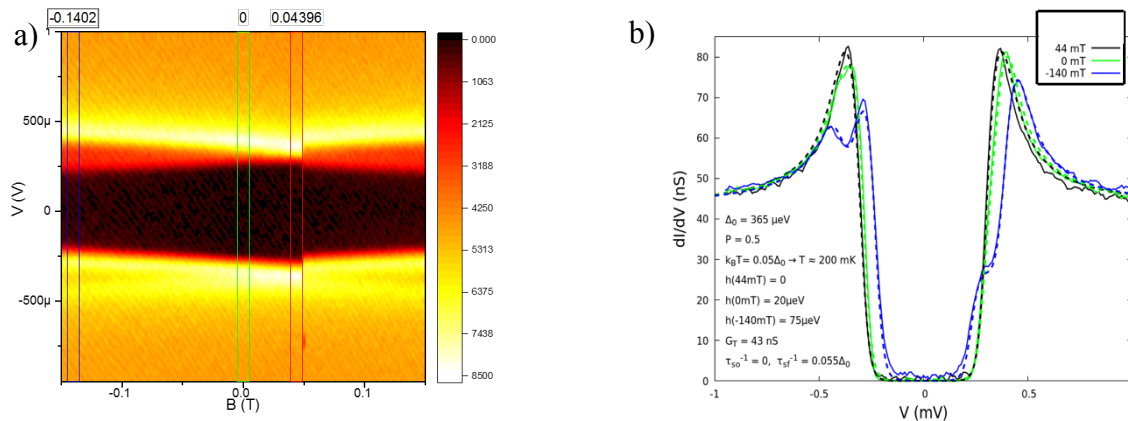


Figure 4. (a) Full evolution of the $dI/dV(V)$ from -150 mT to 150 mT. (b) The $dI/dV(V)$ characteristics for selected values of external magnetic fields (solid lines) with the fitting (dashed lines) and the parameters used. Fitting has been performed by PhD student Mikel Rouco from CFM, San Sebastian, Spain with a numerical model discussed in [15].

2.1.4 Voltage drop vs magnetic field: Hysteresis of the EuS magnetization

A finite voltage drop has been observed across the tunnel junction (pinning numbers 5-6) in an open circuit configuration suggesting a thermoelectric signal induced by a spurious thermal gradient (Figure 5) of the experimental set-up. The V drop follows the magnetization hysteresis of the EuS layer. Still, we cannot claim a thermoelectric effect, because also another spurious signal has been observed across the tunnel barrier. Specifically, the bad matching between the impedance of the sample ($R_{\text{tunnel}}(V=0) \sim 1 \text{ G}\Omega$, see Fig. 3b) and the input impedance of the V amplifier ($R_{\text{in}}(V_{\text{amp}}) \sim 1\text{-}10 \text{ G}\Omega$) induces an additional voltage drop that is also dependent on the changing resistance of the junction. This is consistent with a theoretical modeling of the set-up (not in detail here). Improving the experimental set-up with high impedance V amplifiers will avoid the generation of this signal component.

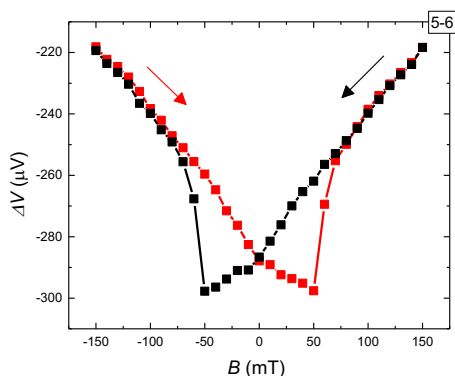


Figure 5. Forward trace (black squares) and backward trace (red squares) of the V drop vs applied magnetic field for the Al/Eu/Cu junction.



2.1.5 Field dependence of the differential conductance at different temperatures

Here, we report the tunneling conductance of the junction extracted from the I - V characteristics acquired in a DC two wire set-up (Fig. 6a), for different bath temperatures T and three values of the applied magnetic field ($B = 0$, $B = 100$ mT, and $B = 150$ mT). The obtained $dI/dV(V)$ curves (Fig. 6b-d) clearly exhibit the conventional tunneling conductance evolution with the T , characterized by a thermal broadening of the peaks and an increasing sub-gap conductance with the increasing of the T .

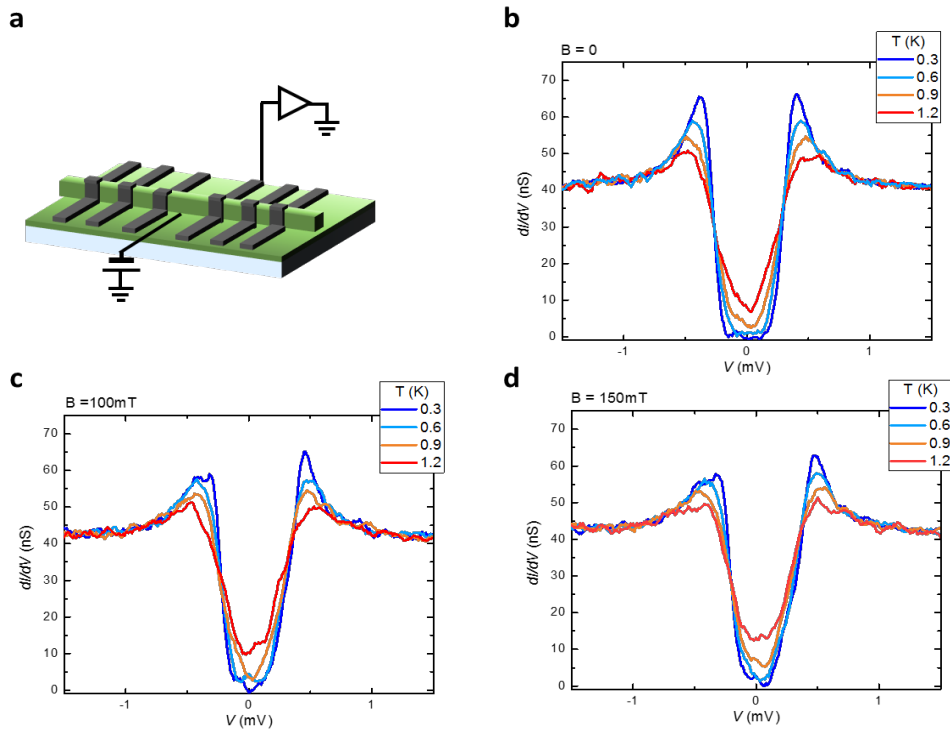


Figure 6. (a) Sketch of the measurement set-up. The $dI/dV(V)$ of the Al/Eu/Cu junction measured at several bath T and (b) at zero magnetic field, (c) $B = 100$ mT, and (d) $B = 150$ mT.

2.1.6 Field dependence of the differential conductance for different heating powers– Non-local heating configuration

In this section, we report the tunneling conductance dependence with the power (P). The measurements are performed by heating the Cu lead in a *non-local configuration*, i.e. with the heat current not intersecting with the probing current path (measurements set-up sketched in Figure 7a). This configuration allows the tunneling spectroscopy of the junctions without interference with the heating circuit. From the measurements, reported in Figures 7b-d for different values of external magnetic field, we observe a net broadening of the conductance consistent with an increase of the average T , while any shift in the voltage drop due to the thermoelectric effect is visible. This



indicates that the non-local heating configuration is not effective in generating a sizable thermal gradient across the junction.

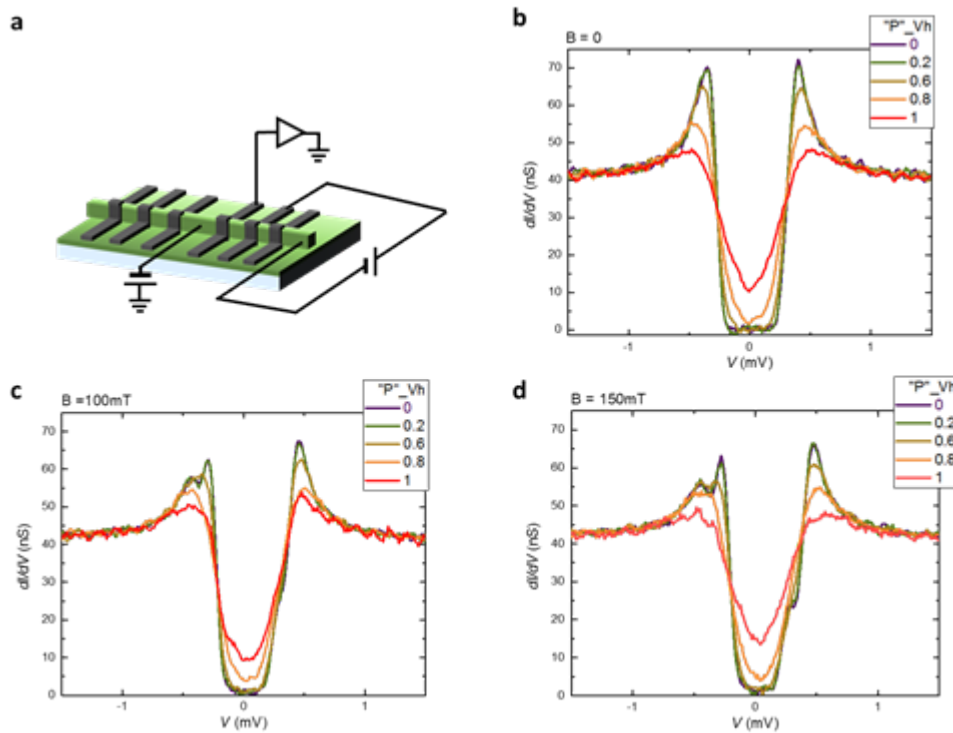


Figure 7. (a) Schematic view of the set-up for non-local measurements. The $dI/dV(V)$ vs V_{bias} of the junction measured at several P and (b) at zero magnetic field, (c) $B = 100$ mT, and (d) $B = 150$ mT (d).

2.1.7 Comparison between temperature and power dependences

From the comparison of the tunneling conductance dependence with T and P (Figure 8) and the good matching between the curves, we conclude that the effect of the non-local heating is a net increase of the sample T , while the effect of the thermal gradient remains difficult to observe suggesting that a different scheme for heating is required to enhance the thermal gradient across the junction.



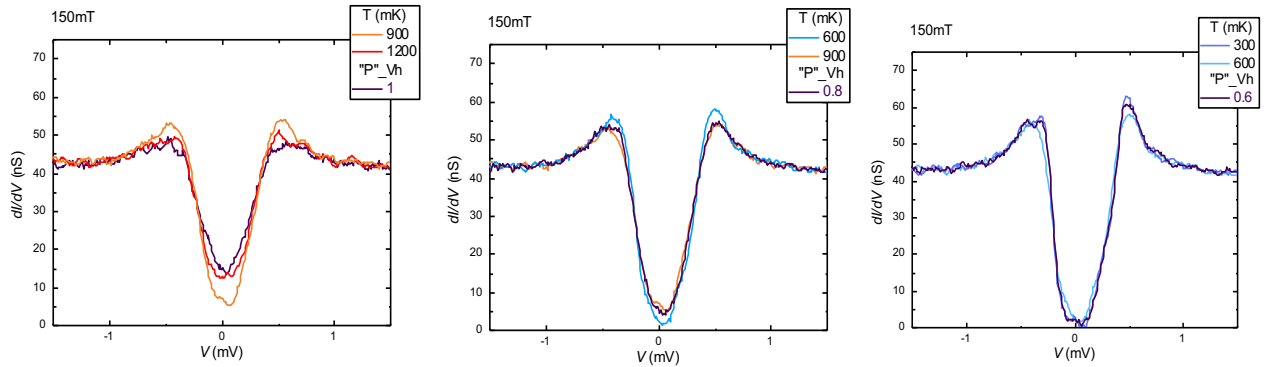


Figure 8. Comparison between temperature and P dependences of the tunneling spectroscopy of the Al/EuS/Cu junction.

2.2 Sample 10222-20Å/A

The sample consists of cross bars fabricated by electron-beam shadow mask evaporation (Figure 9). The typical area of Cu/EuS/Al junction is $300 \times 300 \mu\text{m}^2$.

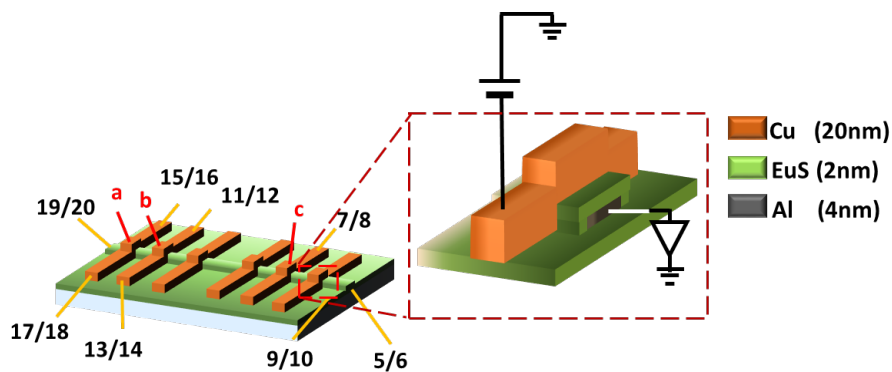


Figure 9. Sketch and measurements set-up of the device investigated with pinning numbers and a magnification of the cross bar forming the Cu/EuS/Al vertical junction.

All the junctions tested show a normal state resistance of $\sim 100 \Omega$ ($R_a = 40 \Omega$, $R_b = 184 \Omega$, and $R_c = 580 \Omega$), consistent with the thinner EuS tunnel barrier. The linear I - V characteristics observed in the low T measurements shown in Figure 10 are incompatible with a tunnel barrier and indicate the presence of pinholes. This makes impossible to perform tunneling spectroscopy in this family of devices.



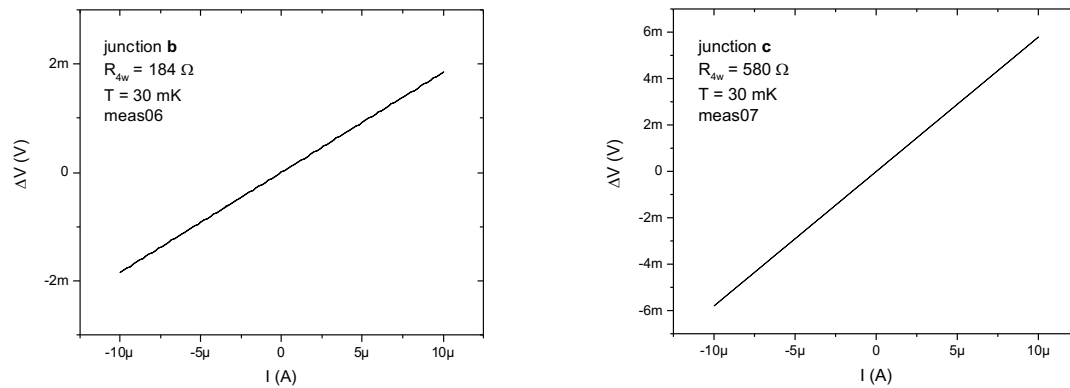


Figure 10. I - V curves for b (left) and c (right) junction. Junctions are labelled on the map of Figure 9.

2.3 Conclusion

Sample 10222-20Å/A (Cu(13 nm)/EuS(2nm)/Al(4nm)) shows no tunneling characteristics in the barrier, compatible with a non-uniformity of the 2 nm of EuS thin film.

Sample 10233-40ÅG (Al(4 nm)/EuS(4 nm)/Cu(13 nm)) shows a good tunnel characteristic and a polarization ($\sim 50\%$) suitable for the development of the radiation detector. Unfortunately, the large tunnel barrier is incompatible with the set-up (R in V_{preamp} is too low) and does not allow a direct measurement of the thermoelectric effect. Moreover, the non-local heating measurements show a net heating of the device without a visible thermal gradient across the junction. Local heating configurations are now investigated and show a promising thermoelectric signal and a net thermal gradient. Data are under analysis and are not reported in this public derivable (D2.1) to avoid conflict of interest with a near future scientific publication.

2.4 Next steps (August 2019)

- (1-2 Months) Characterization of the other two device families with the hope of finding a suitable sample with low tunnel resistance ($R_T \ll R_{in}$), but still good spin polarization.
- (2-4 Months) Proposing different layer configurations by substituting the normal layer (Cu) with a Ferromagnetic material (F) and AlO_x for the tunnel barrier EuS/Al/ AlO_x /Co to improve the quality and conductance of the tunnel barrier and maintain a good spin filtering.

3. CSIC samples

In this section, we report the electrical characterization performed on the FI/S and FI/S/FI films provided by Drs. Celia Rogero and Max Ilyn from the CFM, the partner of the consortium. Separate



Deliverable 1.1 ‘Co/Al₂O₃/Al/EuS films’ explains in more detail the sample realization. They consist of two different generation of EuS/Al-based films:

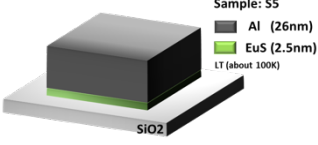
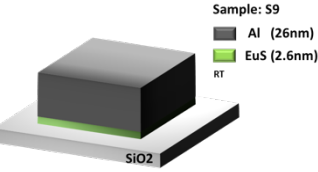
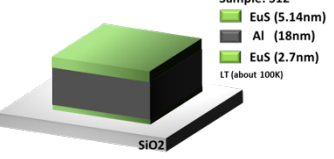
- Generation 1: two films of EuS/Al bilayer (S5, S9) and one EuS/Al/EuS trilayer (S12).
- Generation 2: two of Al/EuS bilayers on a thick Au layer (2L1, 2L3) and one EuS/Al/EuS trilayer (3L3).

We have acquired the temperature (T) dependence of the sheet resistance (R) of the films in order to obtain the value of the critical temperature (T_c) of the superconducting layer. The value of the magnetoresistance at $T \sim T_c$ allows to establish the presence of the EuS in the FI/S and FI/S/FI films, an essential step to demonstrate the magnetic proximity of the EuS layer and select the best growth protocol for high quality FI/S heterostructures.

3.1 Generation 1: samples S5, S9, S12

The fabrication characteristics of samples are given in Table 2.

Table 2. Overview of the fabrication characteristics

Sample	Materials/thicknesses	Sketch of the samples
S5	Al(26 nm)/EuS(2.5 nm)/SiO ₂	
S9	Al(26 nm)/EuS(2.6 nm)/SiO ₂	
S12	EuS(5.14 nm)/Al(18 nm)/EuS(2.7 nm)/SiO ₂	

The bilayer and trilayer structures are compared to test the detrimental effect of the EuS film on the superconductivity of the Al layer.



3.1.1 T dependence of samples S5, S9, S12

Here, we report the temperature dependence of the sheet resistance in order to determine the critical temperature (T_C) of the superconducting film as a function of the thickness and polarization of the FI layer. The measurements are performed in voltage bias and in a DC four wire set-up. As shown in Figure 11, superconductivity is clear visible (T_C (S5) = 2.3 K, T_C (S9) = 1.7 K). The magnetoresistance of the two devices measured at $T \sim T_C$ showed any magnetic hysteresis of the EuS layer indicating a weak coupling between the two layers.

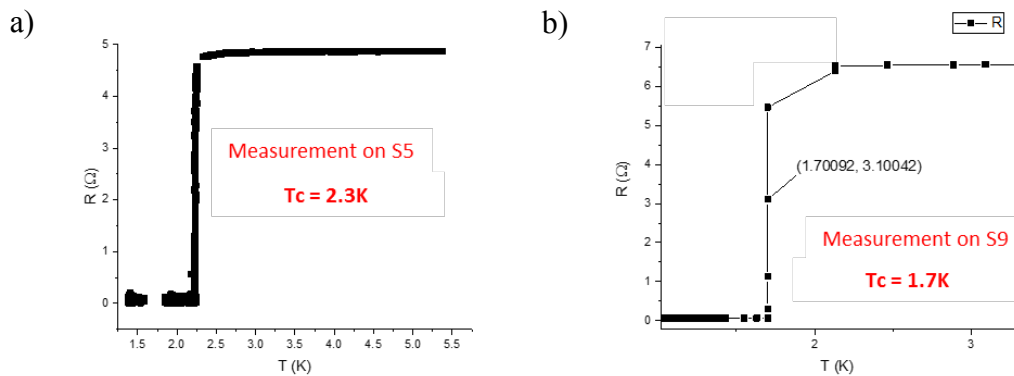


Figure 11. Transition curves for (a) S5 and (b) S9 samples.

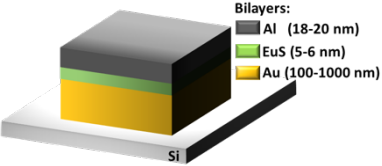
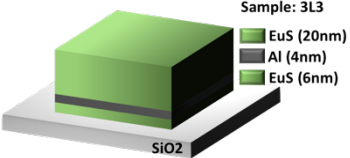
On the contrary, tests on the S12 trilayer didn't show superconductivity of the film down to 25 mK. This indicates that a too strong magnetic proximity effect is present in this sample, killing superconductivity altogether.

3.2 Generation 2: samples 2L1, 2L3 and 3L3

The fabrication characteristics of the Generation 2 of samples are reported in Table 3.



Table 3. Overview of the fabrication characteristics.

Sample	Materials/thicknesses	Sketch of the samples
2L1 2L3	Al(18-10 nm)/EuS(5-16 nm)/Au-thick/Si	
3L3	EuS(20 nm)/Al(4nm)/EuS(6 nm)/SiO ₂	

Samples 2L1 and 2L3 consist of a Au/EuS/Al bilayer. The Au is grown to provide a flat layer in order to improve the quality of the EuS film. The sample 3L3 is a EuS/Al/EuS trilayer in which the thickness of the Al film has been lowered to improve the superconductivity of the layer respect to the first generation of samples. As for the Generation 1, we have measured the sheet resistance trend with the temperature to derive the critical temperature of the superconducting film and the magnetoresistance at $T \sim T_c$ in order to establish the presence of the EuS in the samples.

3.2.1 Sample 2L1

Here, we present the transition curves for sample 2L1, performed in current bias in AC four-wire set-up. As shown in Figure 12, sample shows superconductivity, with a $T_C = 1.7$ K.

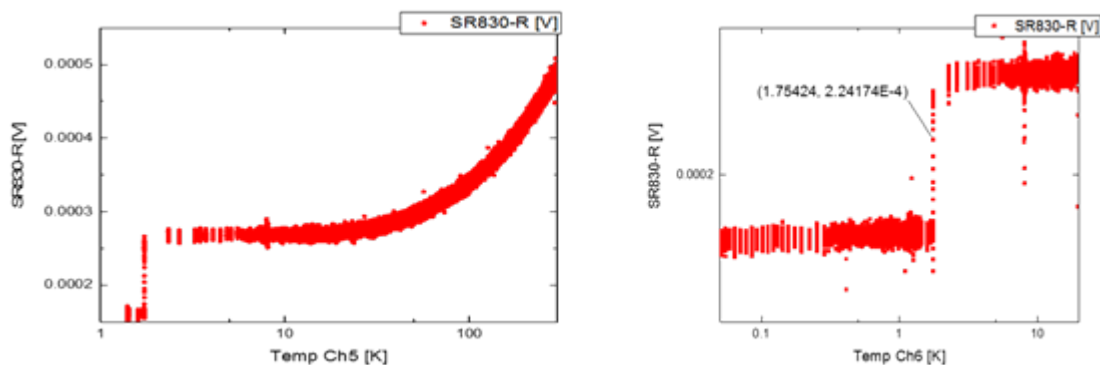


Figure 12. R vs T for sample 2L1. Panel (b) is a zoom of (a) in the transition zone.



3.2.2 Sample 2L3

In this section, we report the measurement performed on the sample 2L3. From the R vs T (Figure 13a) we extract $T_C = 1.7$ K, consistent with the thickness of the Al layer. Moreover, the magnetoresistance of the film, measured just above the T_C (Figure 13b) shows a hysteretic behavior with a dip of resistance at ± 4 mT as expected for a spin split superconductor [13], with a switching field of 4 mT corresponding to the coercive field of the EuS layer. This shows the coexistence of magnetism and superconductivity in the sample 2L3.

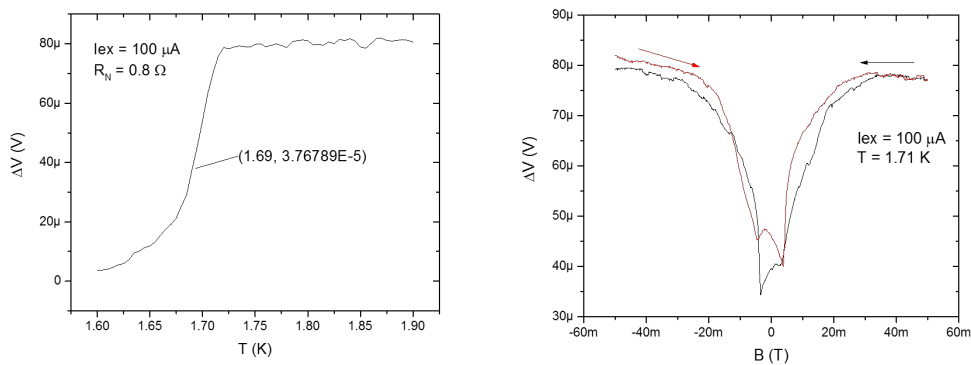


Figure 13. (a) R vs T measure in a DC four wire configuration. (b) Forward and back forward V drop dependence with magnetic field at a constant current bias.

3.2.3. Sample 3L3

From the temperature dependence of the film any superconducting transition is not visible also for this trilayer structure. Probably, the strong exchange energy induced in these multi-layer devices is larger than the Chandrasekhar-Clogston limit ($\hbar > \Delta_0/\sqrt{2}$) [14]. Still, differing from the first generation, some signatures of superconductivity are visible in the non-linearities of the low temperatures I - V characteristic (Figure 14a). This is clear in the differential conductance of the film (Figure 14b) showing a small damping at zero bias consistent with the tunneling spectroscopy of a superconductor with a $\Delta_0 \sim 200$ μ eV compatible with the Al superconducting gap. By following this signal in the in-plane magnetic field a clear hysteretic evolution can be observed in the magnetic field (Figure 14c) suggesting an interaction between the Al DOS and the EuS layers.



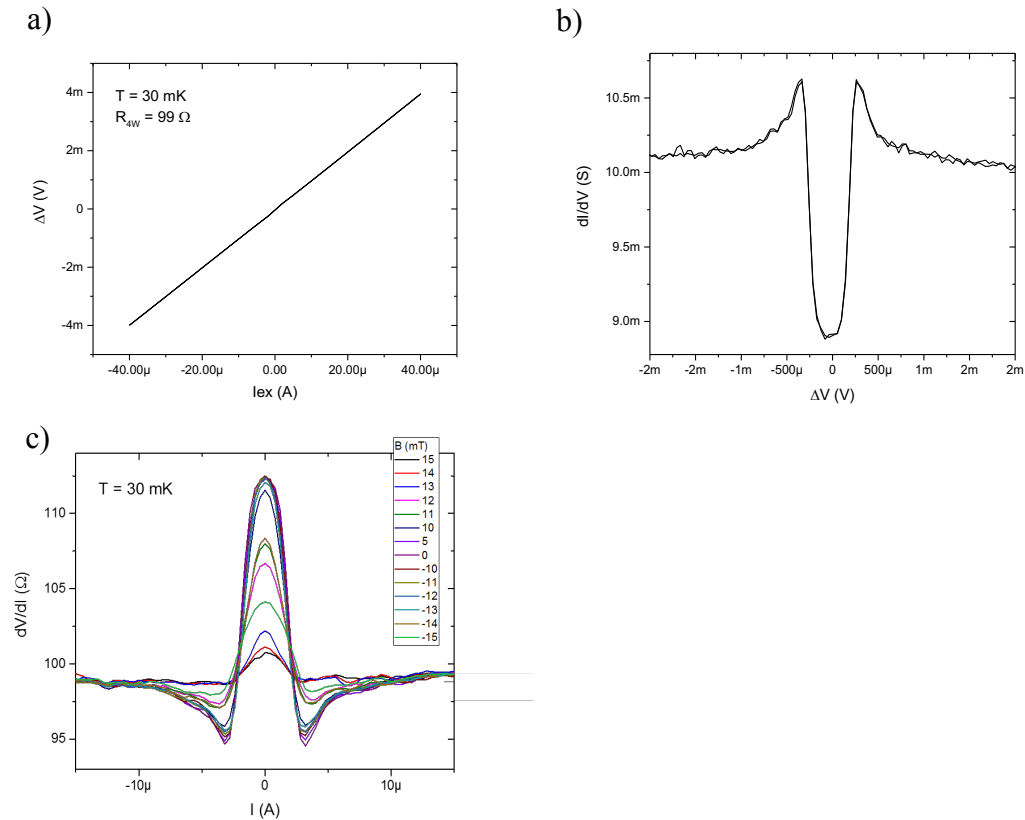


Figure 14. (a) I - V curve measured in the film in a DC four-wire configuration at 30 mK, (b) $dI/dV(V)$ differential conductance extracted from (a) and evolution of dV/dI with an applied magnetic field from 15mT to -15mT.

3.3 Conclusion

The samples grown by CFM showed clear superconductivity in the FI/S bilayer up to ~ 1.7 K. Improvements from the first to the second generation of bilayers have been observed with superconductivity and magnetism on the same film. The magnetization induced by the EuS layer is demonstrated in the hysteretic magnetoresistances of the film suggesting a coercive field of 4 mT.

Moreover, the quenching of superconductivity observed in the trilayer structures FI/S/FI confirms the good coupling between the Al and the EuS layer, inducing an exchange interaction stronger than the superconducting correlations. For lower Al thicknesses precursors of superconductivity are visible in the non-linearity of the differential conductance.

3.4 Next steps (August 2019)

- (1-2 Months) Tunnel barrier is now requested for the tunneling spectroscopy and the quantification of the exchange field induced in the Al layer and the demonstration of the spin filtering of the EuS layer.



This project has received funding from the European Union's Horizon 2020 research and innovation programme under grant agreement No 800923.

- (3-6 Months) More sophisticated devices are now requested for the integration of local heaters and thermometers.
- (4-8 Months) Tunnel junctions capable for the integration of an antenna for the implementation of bolometric detectors.



Bibliography

- [1] R. Meservey, P. M. Tedrow, Spin-polarized electron tunneling, Phys. Rep.238 (4) (1994).
- [2] T. Tokuyasu, J. A. Sauls, D. Rainer, Proximity effect of a ferromagnetic insulator in contact with a superconductor, Phys. Rev. B 38 (1988).
- [3] X. Hao, J. S. Moodera, R. Meservey, Spin-filter effect of ferromagnetic europium sulfide tunnel barriers, Phys. Rev. B 42 (1990).
- [4] P. Tischer, Ferromagnetic domains in EuS investigated by low-temperature Lorentz microscopy, IEEE Trans. Magn. 9 (1973).
- [5] R. Meservey, P. M. Tedrow, Spin-polarized electron tunneling, Phys. Rep. 238 (1994).
- [6] P. M. Tedrow, J. E. Tkaczyk, A. Kumar, Spin-polarized electron tunneling study of an artificially layered superconductor with internal magnetic field: EuO-Al, Phys. Rev. Lett. 56 (1986).
- [7] Xiong, Y M, S. Stadler, P. W. Adams, and G. Catelani, Spin-resolved tunneling studies of the exchange field in EuS/Al bilayers, Phys. Rev. Lett.106 (2011).
- [8] E. Strambini, V. N. Golovach, G. De Simoni, J. S. Moodera, F. S. Bergeret, and F. Giazotto, Revealing themagnetic proximity effect in eus/al bilayers through superconducting tunneling spectroscopy, Phys. Rev. Materials 1 (2017).
- [9] G. De Simoni, E. Strambini, J.S. Moodera, F.S. Bergeret, and F. Giazotto, Toward the Absolute Spin-Valve Effect in Superconducting Tunnel Junctions, Nano Lett. 18 (2018).
- [10] R. Meservey, P.M. Tedrow, Spin-Polarized Electron Tunneling. Phys. Rep. 4 (1994).
- [11] J.S. Moodera, X. Hao, G.A. Gibson, R. Meservey, Electron-Spin Polarization in Tunnel Junctions in Zero Applied Field with Ferromagnetic EuS Barriers, Phys. Rev. Lett. 61 (1988)
- [12] X. Hao, J.S. Moodera, R. Meservey, Thin-Film Superconductor in an Exchange Field, Phys. Rev. Lett. 67 (1991).
- [13] B. Li, N. Roschewsky, B. A. Assaf, M. Eich, M. Epstein-Martin, D. Heiman, M. Münzenberg, and J. S. Moodera, Superconducting Spin Switch with Infinite Magnetoresistance Induced by an Internal Exchange Field, Phys. Rev. Lett. 110 (2013).
- [14] B. S. Chandrasekhar, A note on the maximum critical field of high-field superconductors, Appl. Phys. Lett. 1 (1962).
- [15] Mikel Rouco, Subrata Chakraborty, Faluke Aikebaier, V. N. Golovach, Elia Strambini, Jagadeesh S. Moodera, Francesco Giazotto, Tero T. Heikkilä, F. Sebastian Bergeret, Charge transport through spin-polarized tunnel junction between two spin-split superconductors, arXiv:1906.09079.



Appendix 1

Summary of changes of this deliverable after first review meeting:

- Figures and Tables are changed: sketch of the samples modified to show the real coverage of the EuS layer;
 - o Table 1, sketches are changed
 - o Figure 1, sketch is changed
 - o Figures 6, 7 & 9 sketches are changed
 - o Figure 11 is changed
 - o Table 3, sketches are changed
 - o Figure 12 is changed
 - o Figure 14 is changed
- Section 2: more details on experiment in the introduction;
- Section 2.1.1: more details on the experimental set-up used and data analysis;
- Section 2.1.2: explanation of the procedure for the magnetization of the EuS;
- Section 2.1.3: detailed description of the dI/dV dependence of the tunnel junction with the applied magnetic field with a discussion on the experimental findings;
- Section 2.1.5: more details about the experimental set-up and data analysis;
- Section 2.1.6: more details about the non-local configuration;
- Section 2.2: considerations on the experimental results;
- Section 2.3: conclusion section moved from 2.1.8 to 2.3, and anticipations on the present experiments on the thermoelectric effect include;
- Section 3: included more details in samples description;
- Section 3.1.1: more details about the results
- Section 3.2: detailed description of the fabrication characteristics
- Section 3.2.3: more comments on the experimental results included;
- Section 3.3: included in the conclusions a deeper discussion on the experimental findings.

